DET NORSKE VIDENSKAPS-AKADEMI I OSLO

GEOFYSISKE PUBLIKASJONER
GEOPHYSICA NORVEGICA

Vol. XXVIII. No. 3 December 1971

ARNT ELIASSEN AND JAN-EDGAR REKUSTAD

A Numerical Study of Meso-Scale Mountain Waves

OSLO 1971
UNIVERSITETSFORLAGET

GEOFYSISKE PUBLIKASJONER
GEOPHYSICA NORVEGICA
VOL. XXVIII NO. 3

A NUMERICAL STUDY OF MESO-SCALE MOUNTAIN WAVES

By
Arnt Eliassen and Jan-Edgar Rekustad

FREMLAGT I VIDENSKAPS-AKADEMIETS MØTE DEN 19. MARS 1971

Summary. Numerical integrations are performed of the equations describing air flow on the rotating earth across a mountain ridge with a width of about 400 km. The motion is assumed to be hydrostatic and independent of the y coordinate (along the ridge). A nearly steady state is reached after 34 hours, showing a system of meso-scale gravity-inertia waves which are strongly damped downstream. In the case of relatively weak static stability, the maximum lifting of the isentropic surfaces occurs on the lee side of the ridge at an altitude of about 5 km.

1. Introduction. The effect of ground topography on the air motion presents a problem with many aspects. Ground corrugations with a horizontal scale of the order 10 km give rise to the familiar short gravity mountain waves, which often lead to formation of lenticular clouds, or to modifications of the shape of pre-existing cloud layers. On the other end of the spectrum, there is the long Rossby-type mountain waves set up by the extensive continental mountain ranges. The present paper deals with the meso-scale gravity-inertial mountain waves caused by ground corrugations of the scale 100—1000 km. These waves are strongly influenced by the rotation of the earth, but they are not quasi-geostrophic. They may be quite important for the distribution of orographic clouds and precipitation, and may also contribute significantly to the total mountain stress.

To the authors' knowledge, only a few studies of mesoscale mountain waves have been published. Some results concerning the flux of wave energy and momentum in the linearized case have been given by A. Eliassen & Palm (1961), and the effect of the critical wavelength, for which the particle frequency equals the Coriolis parameter, has been studied by Jones (1967) and A. Eliassen (1968).

In the present paper, meso-scale mountain waves in two dimensions are determined by numerical integration of the time-dependent equations until the motion appears to be stationary.

2. The equations in Θ-coordinates. The problem under consideration is to determine, for a straight horizontal flow, the disturbances caused by prescribed corrugations of the underlying ground surface. The horizontal scale of the ground corrugations and the disturbances are assumed to be of the order 100—1000 km, i.e. sufficiently large for the motions to be described by the quasi-static equations, but still small enough for the Coriolis parameter to be considered constant and the curvature of the earth ignored. For velocities of the order 10 ms^{-1}, the corresponding time scale is of the order of a few hours to one day. This is too small for quasi-geostrophic motion, but large enough for the rotation of the earth to be essential; moreover, it is sufficiently small for heat sources to be ignored. The air is assumed to be non-saturated, so that the potential temperature θ is materially conserved.

Using θ as vertical coordinate, and horizontal Cartesian coordinates x, y, the equations expressing change of horizontal momentum, mass continuity, and vertical equilibrium are

$$\frac{\partial u}{\partial t}+u\frac{\partial u}{\partial x}+v\frac{\partial u}{\partial y}-fv+\frac{\partial M}{\partial x}=0 \tag{1}$$

$$\frac{\partial v}{\partial t}+u\frac{\partial v}{\partial x}+v\frac{\partial v}{\partial y}+fu+\frac{\partial M}{\partial y}=0 \tag{2}$$

$$\frac{\partial^2 p}{\partial t\partial\Theta}+\frac{\partial}{\partial x}\left(u\frac{\partial p}{\partial\Theta}\right)+\frac{\partial}{\partial y}\left(v\frac{\partial p}{\partial\Theta}\right)=0 \tag{3}$$

$$\frac{\partial M}{\partial\Theta}=\Pi \tag{4}$$

where

$$\Pi=c_p\left(\frac{p}{p_0}\right)^{\gamma},\quad \gamma=\frac{R}{c_p} \tag{5}$$

is the Exner function, and

$$M=c_pT+gz=\Pi\Theta+gz \tag{6}$$

the Montgomery potential.

The notation is as follows: t time, u, v horizontal velocity components, f (=constant) Coriolis parameter, p pressure, p_0 reference pressure (=1 bar), R gas constant referred to unit mass, c_p specific heat at constant pressure, g acceleration of gravity, z height above sea level.

The geostrophic velocity components will be denoted by U and V:

$$\frac{\partial M}{\partial x}=fV,\quad \frac{\partial M}{\partial y}=-fU \tag{7}$$

The thermal wind equations are obtained by combining (7) and (4):

$$\frac{\partial\Pi}{\partial x}=f\frac{\partial V}{\partial\Theta},\quad \frac{\partial\Pi}{\partial y}=-f\frac{\partial U}{\partial\Theta} \tag{8}$$

or, in terms of p instead of Π

$$\frac{\partial p}{\partial x}=\frac{f}{\gamma}\frac{p}{\Pi}\frac{\partial V}{\partial \Theta}, \quad \frac{\partial p}{\partial y}=-\frac{f}{\gamma}\frac{p}{\Pi}\frac{\partial U}{\partial \Theta} \tag{9}$$

3. Reduction to two spatial dimensions. Generally, the dependent variables are functions of x, y, Θ, and t. We shall here consider the simpler, two-dimensional problem of a horizontally uniform current in the x-direction crossing a ridge in the ground surfaces at right angles. The velocity components may then be assumed to be independent of the y-coordinate:

$$\frac{\partial u}{\partial y}=\frac{\partial v}{\partial y}=0 \text{ for all } t \tag{10}$$

In order that (10) shall remain true for all times, it is necessary that all terms in (1) and (2) are independent of y, i.e.

$$\frac{\partial^2 M}{\partial x \partial y}=f\frac{\partial V}{\partial y}=-f\frac{\partial U}{\partial x}=0, \quad \frac{\partial^2 M}{\partial y^2}=-f\frac{\partial U}{\partial y}=0 \tag{11}$$

so that U is a function of Θ and t only. Using (4), we also find

$$\frac{\partial^2 \Pi}{\partial x \partial y}=\frac{\partial^2 \Pi}{\partial y^2}=0 \tag{12}$$

It will be noted that, as a result of the non-linear relation (5) between Π and p, eq. (3) will not guarantee that (12) remains true at all times; strictly speaking, a baroclinic current will therefore not remain two-dimensional, even if it is so initially. However, the resulting departure from two-dimensionality is slight and will be ignored in this study.

With the simplifications (10) and (11), eqs. (1—4), become

$$\frac{\partial u}{\partial t}+u\frac{\partial u}{\partial x}-fv+\frac{\partial M}{\partial x}=0 \tag{13}$$

$$\frac{\partial v}{\partial t}+u\frac{\partial v}{\partial x}+f(u-U)=0 \tag{14}$$

$$\frac{\partial^2 p}{\partial t \partial \Theta}+\frac{\partial}{\partial x}\left(u\frac{\partial p}{\partial \Theta}\right)-\frac{f}{\gamma}v\frac{\partial}{\partial \Theta}\left(\frac{p}{\Pi}\frac{\partial U}{\partial \Theta}\right)=0 \tag{15}$$

$$\frac{\partial M}{\partial \Theta}=\Pi \tag{16}$$

The last term of (15), where we have made use of the last eq. (9) to eliminate $\partial^2 p/\partial y \partial \Theta$, was dropped in the computations since its effect was found to be negligible.

In eqs. (13—16), u, v, U, and $\partial M/\partial x$ are independent of y, whereas p, Π and M vary with y. However, since no derivatives with respect to y appear, we may apply the equations at some selected constant value y_0 of y. All variables may then be considered as functions of x, Θ, and t only, and the problem is thus reduced to one in two spatial dimensions. The method involves a slight inconsistency, since eqs. (15) and (16) will be slightly different for a different y_0; but this is thought to be of little consequence.

4. Boundary conditions. The surface of the ground is assumed to coincide with an isentropic surface $\Theta=\Theta_G$. The domain of integration may then be taken as a rectangle in the coordinates x, Θ (with a fixed value of y). It is bounded below by the ground $\Theta=\Theta_G$, and above by an isentropic surface $\Theta=\Theta_T$; the upstream and downstream boundaries are vertical lines at $x=x_A$ and $x=x_B$, respectively.

The height of *the ground surface* $\Theta=\Theta_G$ is a prescribed function of x, denoted by $h(x)$, representing the mountain profile. However, it was found convenient to start the integration with a level ground, and let the mountain build up gradually during the first stages of the computation. Thus we set

$$z(x, \Theta_G, t)=\alpha(t)\cdot h(x) \tag{17}$$

where $\alpha(t)$ increases from $\alpha(0)=0$ to $\alpha(t)=1$ when $t\geq t_0$. In terms of the Montgomery potential, the boundary condition at the ground is

$$M(x, \Theta_G, t)=\Theta_G\Pi(x, \Theta_G, t)+g\alpha(t)h(x) \tag{18}$$

This expression serves as a boundary value for integration of the hydrostatic equation (16).

At *the inflow boundary* $x=x_A$, the velocity is given at all levels and at all times. The inflow velocity is assumed to be parallel with the x-axis and equal to the x-component of the geostrophic wind $U(\Theta, t)$,

$$\left.\begin{aligned} u(x_A, \Theta, t)&=U(\Theta, t)\\ v(x_A, \Theta, t)&=0\end{aligned}\right\} \tag{19}$$

Thus U is a prescribed function, whereas no restriction is placed on $V=V(x, \Theta, t)$. In the present study, the inflow velocity is taken to be independent of time, and the first equation (19) reads

$$u(x_A, \Theta, t)=U(\Theta) \tag{20}$$

In addition, the thermal structure of the inflowing air must be defined by prescribing a relation between p and Θ at $x=x_A$. This relation is likewise taken to be independent of time:

$$p(x_A, \Theta, t)=P(\Theta) \tag{21}$$

The upper boundary $\Theta=\Theta_T$ is treated as a free surface with boundary condition

$$p(x, \Theta_T, t)=P(\Theta_T)=\text{constant} \tag{22}$$

This is an artificial condition, its main merit being that it is mathematically consistent. It will cause a spurious reflection of wave energy from the upper boundary; however, this is prevented by introduction of a Rayleigh friction, to be described later.

It is also necessary to formulate boundary conditions at *the outflow boundary* $x=x_B$. The physically consistent form of these conditions is not quite clear. The conditions should be sufficient to close the system of finite difference equations, and should minimize the undesired reflection of wave energy from the outflow boundary.

NITTA (1962) investigated several outflow conditions in the case of an advection equation, and found that the best result was obtained from equating the individual derivative to zero at the outflow boundary, using non-centered, backward differences in time and space. Although the present problem is not quite the same, we have adopted a similar condition, viz:

$$\left.\begin{aligned} &\frac{\partial u}{\partial t}+u\frac{\partial u}{\partial x}=0\\ &\frac{\partial v}{\partial t}+u\frac{\partial v}{\partial x}=0\\ &\frac{\partial p}{\partial t}+u\frac{\partial p}{\partial x}=0 \end{aligned}\right\} \text{ at } x=x_B \tag{23}$$

5. Elimination of spurious wave energy reflection by addition of an artificial friction. The gravity-intertia waves set up by the mountain ridge will transfer wave energy upwards and downstream. Some of the wave energy may be reflected from inhomogeneities in stability and wind conditions at higher levels. In addition, spurious reflection of wave energy must be expected to take place at the artificial upper and outflow boundaries introduced for the sake of computation. In order to eliminate such reflection as far as possible, an artificial friction was introduced near the upper and downstream boundaries, aiming at dissipating most of the wave energy in these regions. The friction was chosen as a "Rayleigh friction", which does not increase the order of the differential equations. Thus eqs. (13) and (14) were replaced by

$$\frac{\partial u}{\partial t}+u\frac{\partial u}{\partial x}-fv+\frac{\partial M}{\partial x}+\kappa(u-U)=0 \tag{24}$$

$$\frac{\partial v}{\partial t}+u\frac{\partial v}{\partial x}+f(u-U)+\kappa v=0 \tag{25}$$

The coefficient κ was put equal to zero everywhere except near the upper and downstream boundaries.

6. Initial conditions. The objective of the calculation is to determine steady wave patterns in relation to the temperature and wind profiles of the air current. This is done by computing the evolution of the motion in time, starting from a chosen initial

state, until it no longer changes noticeably. The underlying assumption is that the final steady state does not depend on the initial condition, but only on the boundary conditions. The initial condition is thus immaterial, provided that it does not lead to wave breaking during the transient stage, which might cause the numerical integration to break down.

As explained in section 4, we chose to start with a straight horizontal current over level ground and let the mountain build up during the first stages of the computation, as expressed by the boundary condition (17). The initial condition is thus

$$\left.\begin{aligned} u(x, \Theta, 0) &= U(\Theta) \\ v(x, \Theta, 0) &= 0 \\ p(x, \Theta, 0) &= P(\Theta) \end{aligned}\right\} \tag{26}$$

7. Finite difference equations. A square grid in the $x\Theta t$-space is defined by

$$\left.\begin{aligned} x_i &= i\Delta x\,, \quad i=0, 1, \ldots, \mathrm{I} \\ \Theta_j &= \Theta_G + j\Delta\Theta\,, \quad j=0, 1, \ldots, \mathcal{J} \\ t_k &= k\Delta t\,, \quad k=0, 1, \ldots \end{aligned}\right\} \tag{27}$$

The values of u, v, p and M in the grid points are denoted by $u_{i,j,k}$ etc. They are arranged in a staggered chessboard-pattern in the xt-plane, so that u, p, and M are defined in points where $i+k$ is even, and v in points where $i+k$ is odd, as shown in Fig. 1. There is no staggering in the vertical; in other words, Fig. 1 applies to any value of j. The finite difference analogues of (13—16) are formulated as follows, using the leap-frog scheme, and with $2\Delta x$ as unit of length, $2\Delta t$ as unit of time, and p measured in bars,

$$u_{i,j,k+1} - u_{i,j,k-1} = -\tfrac{1}{2}(u^2{}_{i+1,j,k} - u^2{}_{i-1,j,k}) + fv_{i,j,k} - M_{i+1,j,k} + M_{i-1,j,k}$$

$$v_{i+1,j,k+1} - v_{i+1,j,k-1} = -u_{i+1,j,k}(v_{i+2,j,k} - v_{i,j,k}) - f(u_{i+1,j,k} - U_j)$$

$$\begin{aligned} p_{i,j,k+1} - p_{i,j-1,k+1} &= p_{i,j,k-1} - p_{i,j-1,k-1} \\ &+ \tfrac{1}{2}(u_{i+1,j-1,k} + u_{i+1,j,k}) \cdot (p_{i+1,j-1,k} - p_{i+1,j,k}) \\ &- \tfrac{1}{2}(u_{i-1,j-1,k} + u_{i-1,j,k}) \cdot (p_{i-1,j-1,k} - p_{i-1,j,k}) \end{aligned}$$

$$M_{i+1,j,k} - M_{i+1,j-1,k} = \frac{c_p \Delta\Theta}{2}(p^\gamma_{i+1,j,k} + p^\gamma_{i+1,j-1,k}) \tag{28}$$

As mentioned before, the last term of (15) was dropped because it was found to have a negligible effect.

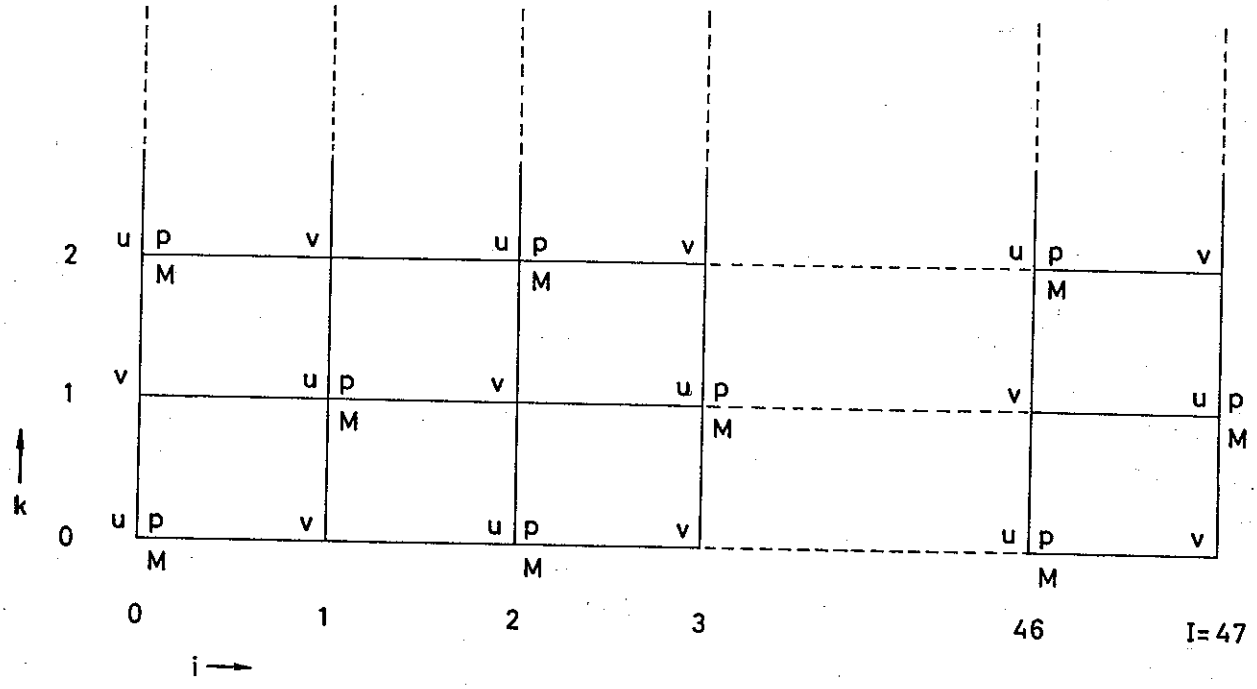

Fig. 1. Staggering of gridpoints in the xt-plane.

The boundary conditions (18—23) are written as follows

$$\left.\begin{aligned} &M_{i,0,k}=\Theta_G\Pi_{i,0,k}+g\alpha_k h_i \quad (j=0)\\ &\left.\begin{aligned} &u_{0,j,k}=U_j\\ &v_{0,j,k+1}=0\\ &p_{0,j,k}=P_j \end{aligned}\right\} \ (i=0\,,\ k \text{ even})\\ &p_{i,J,k}=P_J \qquad (j=\mathcal{J}) \end{aligned}\right\} \tag{29}$$

The initial conditions are

$$\left.\begin{aligned} &u_{i,j,0}=u_{i+1,j,1}=U_j\\ &v_{i+1,j,0}=v_{i,j,1}=0\\ &p_{i,j,0}=p_{i+1,j,1}=P_j \end{aligned}\right\} \ (k=0.1) \tag{30}$$

In order to suppress false solutions permitted by the leap-frog method, the following smoothing was performed at points next to the inflow boundary: $u_{1,j,k}$ was replaced by $\frac{1}{2}(u_{1,j,k}+U_j)$, and likewise for v and p; moreover, $u_{2,j,k+1}$ was replaced by $\frac{1}{3}(2u_{2,j,k+1}+u_{1,j,k})$. This procedure effectively damped out noise waves of wave length $2\Delta x$.

8. Numerical values of parameters. The calculation was intended to simulate a westerly air flow across the Scandinavian mountain range; therefore the value of the Coriolis parameter at 65° latitudes was used ($f=1.33\times10^{-4}\mathrm{s}^{-1}$). The calculations were made for a grid of 48×24 gridpoints in the $x\Theta$-plane, i.e. $I=47$, $\mathcal{J}=23$. The mesh-sizes were:

$$\Delta x=25\ \mathrm{km}\,,\quad \Delta t=55\ \mathrm{s}$$

The latter is dictated by the *CFL* stability criterion.

In the vertical, a variable $\Delta\Theta$ was used in order to get suitable resolution in the troposphere as well as in the stratosphere.

In this paper, results for two different temperature profiles are presented. Case *a* has a relatively strong overall static stability, and case *b* a weak static stability. In case *a*:

$$\Theta_G=263^\circ\mathrm{K},\ \Delta\Theta=\begin{cases}2.5^\circ, & 0<j<6\\ 5^\circ\ , & 6<j<15\\ 10^\circ\ , & 15<j<23\end{cases}$$

In case *b*:

$$\Theta_G=283^\circ\mathrm{K},\ \Delta\Theta=\begin{cases}1.25^\circ\mathrm{K}\,, & 0<j<6\\ 2.5^\circ\mathrm{K}\ , & 6<j<15\\ 5^\circ\mathrm{K}\ , & 15<j<23\end{cases}$$

Fig. 2 shows the values of Θ_j and U_j plotted as functions of P_j for the two cases. (It will be noticed that the values of U_j are the same in cases *a* and *b*.) U_j is increasing all the way to the top, as is often the case in midwinter. Also shown is a wind profile (*b'*) which coincides with profile *b* up to 300 mb, has a strong jet maximum at about 250 mb, and then decreases upward in the stratosphere.

The adjustment time of the bottom profile was set to $t_0=16$ hours (i.e. $\alpha(t)=1$ when $t>16$ hours, eq. (17)).

The coefficient of Rayleigh friction κ was given the following values near the upper boundary (in the unit $10^{-4}\mathrm{s}^{-1}$):

j	23	22	21	20	19	18	17	16	15 etc.
κ	12.5	6.7	3.6	2.0	1.1	0.6	0.3	0.17	0

Near the outflow boundary, the following values were used:

i	46	45 – 44	43 – 42	41 etc.
κ	3.0	1.5	0.75	0

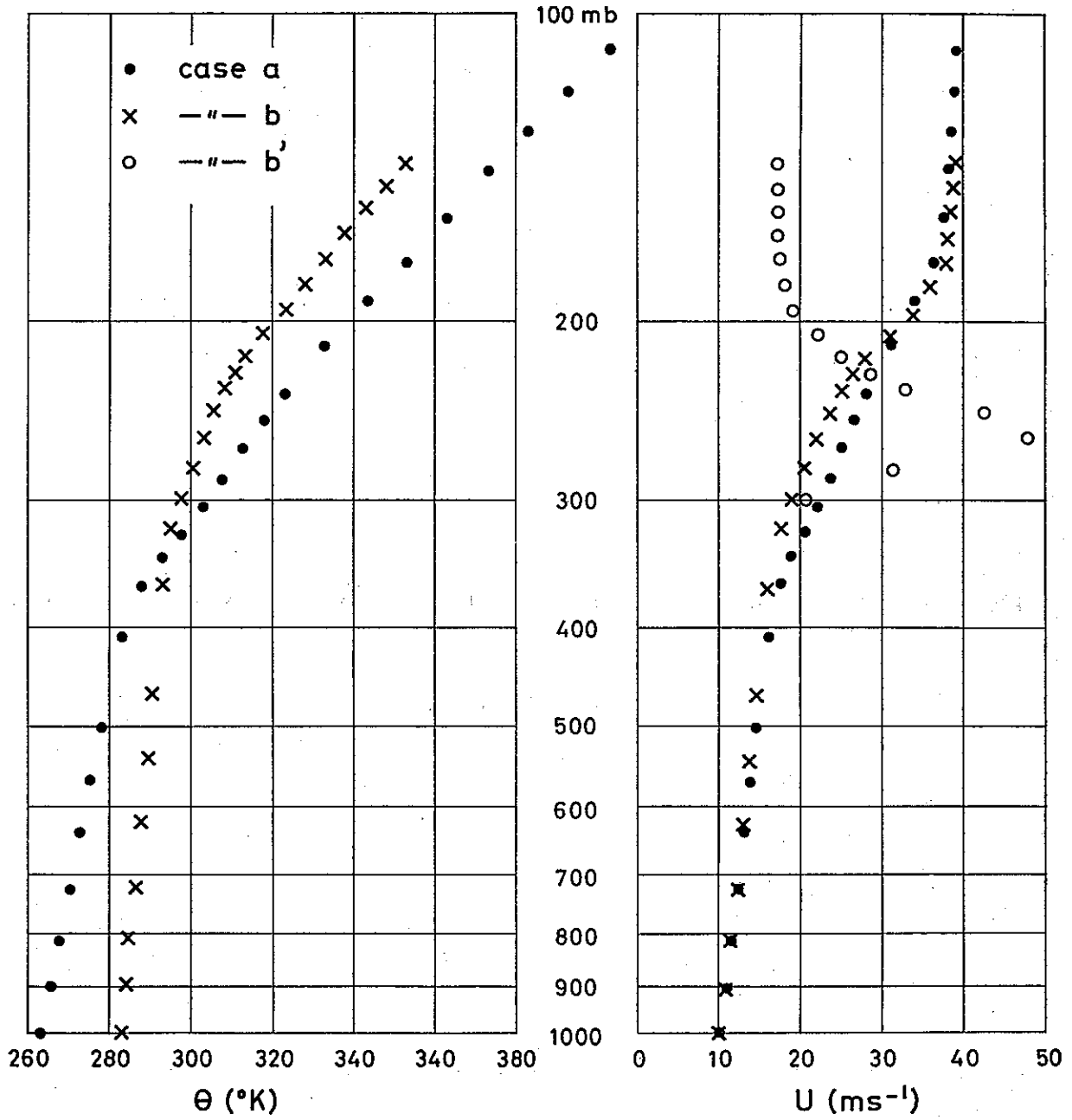

Fig. 2. Potential temperature and wind profiles. Case a: Strong static stability; case b: Weak static stability; case b': Weak static stability with a strong wind maximum near the tropopause.

9. Results. Figs. 3—7 show the location of selected isentropic surface in the *xz*-plane after 34.4 hours (1127 double time steps). At this stage the fields appeared to be very nearly stationary; the computation was in some cases carried to beyond 50 hours without noticeable change.

In Figs. 3 and 4, the same mountain profile of height 890 m was used. Fig. 3 is calculated from the temperature and wind profiles of case *a* in Fig. 2 (strong static stability), and Fig. 3 from case *b* (weak static stability).

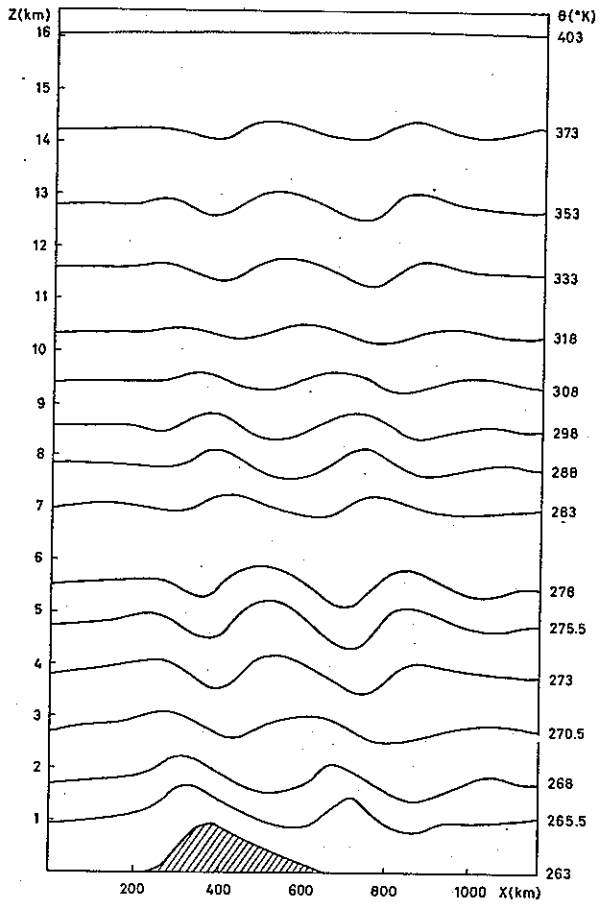

Fig. 3. Vertical cross-section along the flow (*xz*-plane) after 34.4 hours, showing mountain profile and the location of selected isentropic surfaces. Case a: Strong static stability.

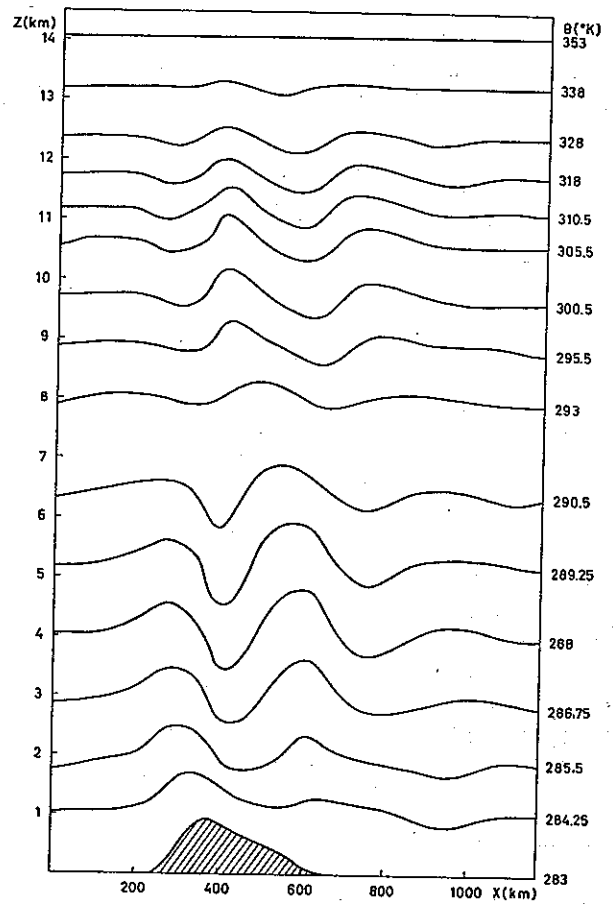

Fig. 4. Same as Fig. 3. Case b: Weak static stability.

In both cases, a crest appears in the lower troposphere above the windward mountain slope, and another crest 3—400 km downstream. These crests, as well as the trough between them, tilt upstream with height, showing that wave energy is transferred upward and momentum downward, in agreement with linear theory (ELIASSEN & PALM 1961).

The total horizontal pressure force exerted on the mountain was computed in both cases; as one would expect, the force decreases with decreasing static stability. Its value was 1.40×10^5N m^{-1} in the case shown in Fig. 3, and 0.97×10^5N m^{-1} in the case shown in Fig. 4.

In case *a* (strong static stability, Fig. 3), the vertical wave amplitudes are moderate, with a maximum of about 500 m in the mid-troposphere. The tilt of the waves is strong. At about 4 km height, the first crest disappears, and a third crest appears further downstream; and at about 10 km height the second crest disappears and a fourth crest appears. There is a quick damping of the waves towards the downstream boundary.

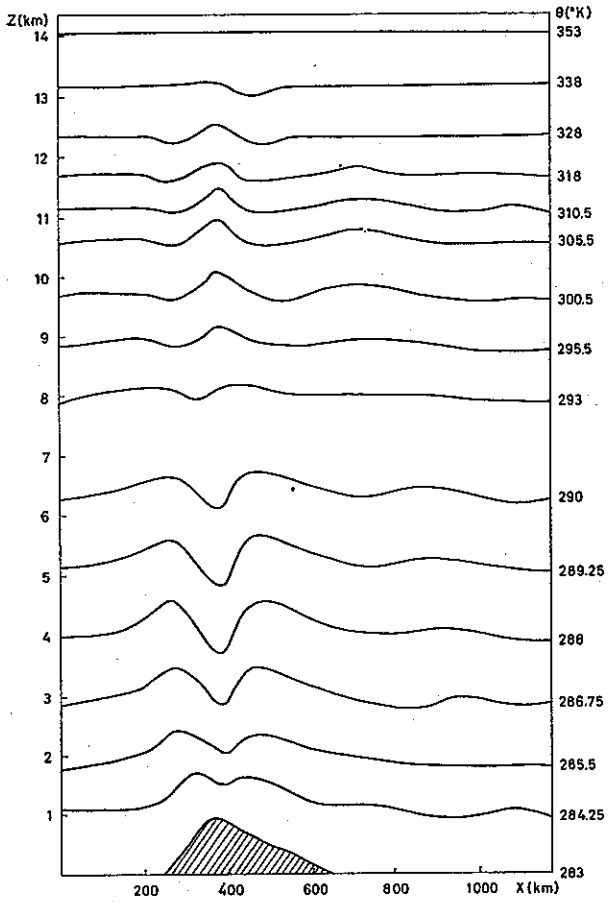

Fig. 5. Same as Fig. 3. Case b: Weak static stability, equations linearized.

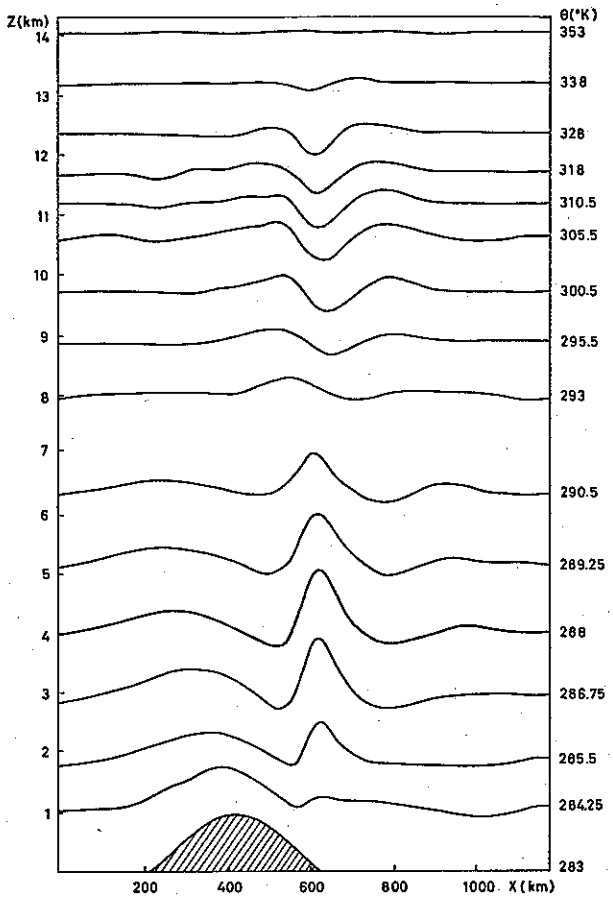

Fig. 6. Same as Fig. 3. Case b: Weak static stability, symmetric mountain profile.

In case *b* (Fig. 4), the wave pattern again tilts upstream with height, but the tilt is much weaker. In the stratosphere, the first crest has disappeared, and a third crest shows up.

The most noteworthy difference between cases *a* and *b* is in the wave amplitude. In case *b* the strongest lifting of the isentropic surfaces from their upstream levels is found in mid-troposphere (4—5 km) in the second wave crest, located over the lee slope of the mountain ridge; its maximum value is about 1000 m. If the incoming air is sufficiently humid, the lifting should be sufficient for formation of a stationary wave cloud with a breadth of the order 100 km. But even if the lifting in these meso-scale mountain waves is insufficient for producing condensation, it may cause an increase in the relative humidity which is sufficient for superimposed short gravity mountain waves to show up as wave clouds. Thus the meso-scale wave pattern may determine preferred areas for appearance of gravity wave clouds.

The cross-section shown in Fig. 5 has been computed from linearized equations; the mountain shape, the velocity profile and the temperature profile are as in Fig. 4 (case b), and the difference between Figs. 4 and 5 is therefore only due to the lineariza-

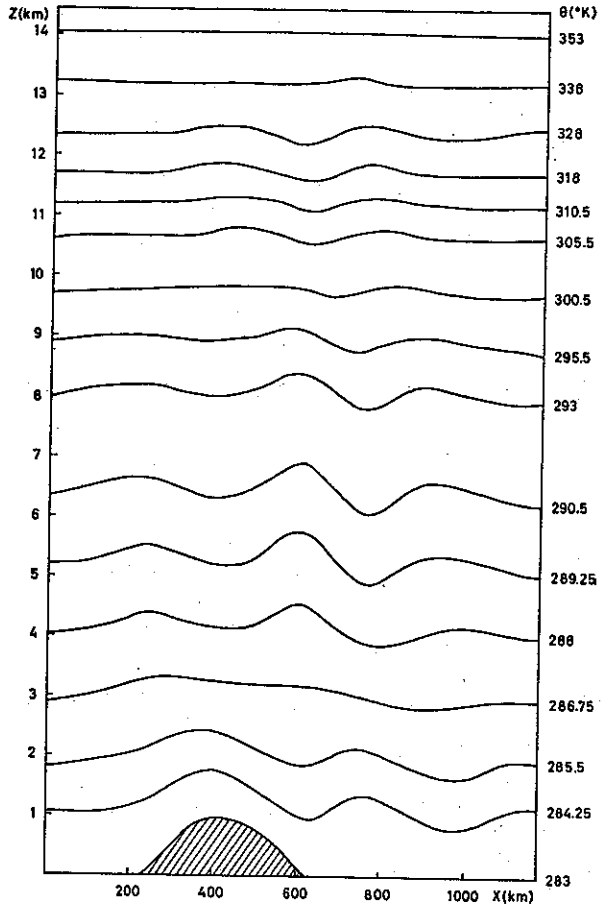

Fig. 7. Same as Fig. 3. Case b': Weak static stability with a wind jet. Symmetric mountain profile.

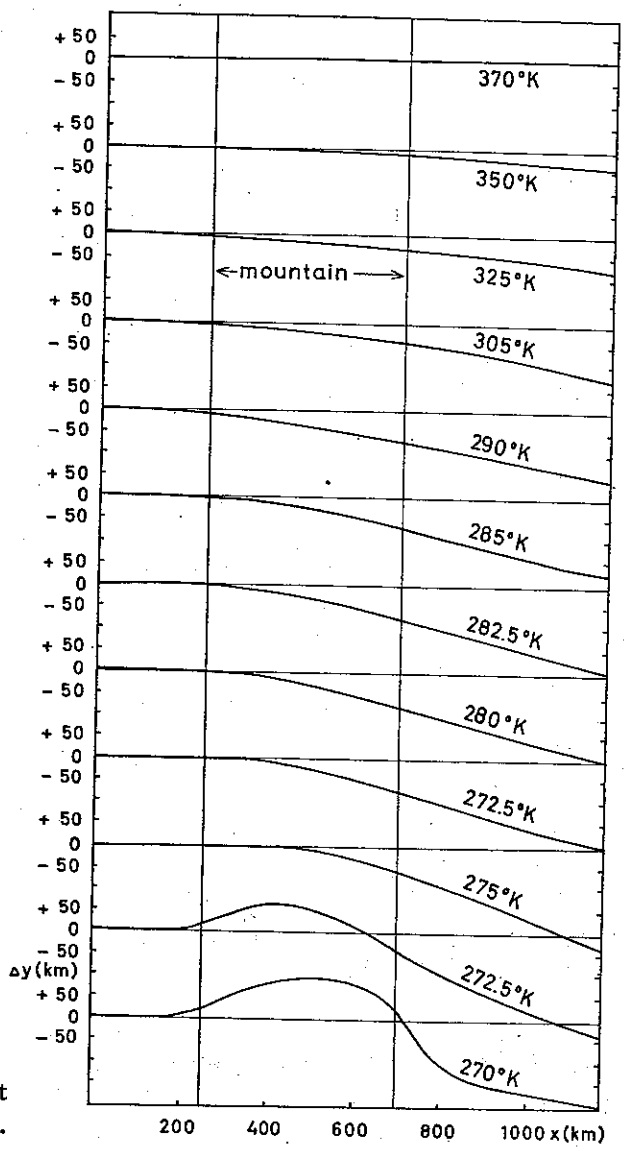

Fig. 8. Streamlines in horizontal projection at different levels, for a case similar to the one shown in Fig. 3.

tion. It will be seen that the linearized equations in this case give much smaller wave amplitudes and a stronger downstream damping.

Fig. 6 is again computed from the non-linear equations, but with a somewhat different mountain profile, shaped as a sine-curve with crest height 850 m; otherwise all conditions are as in Fig. 4 (case b). Comparison between Figs. 4 and 6 indicates that the wave pattern is quite sensitive to changes in the mountain profile. However, in Fig. 6 we refind the high crest in mid-troposphere over the lee slope of the mountain.

In Fig. 7, the conditions are identical with those of Fig. 6, except for a change in the wind profile above 300 mb, as indicated by *b'* in Fig. 2. Thus the wind profile corresponding to Fig. 7 has a strong jet maximum at about 260 mb ($\Theta = 303°$, $z = 10$ km). The effect of this jet is seen to be a pronounced suppression of the wave amplitude at all levels, but in particular at the jet level itself.

Fig. 8 shows the horizontal projection of a number of streamlines at different levels, for a case which is similar to the case shown in Fig. 4. At low levels, the streamlines exhibit a cyclonic curvature on the windward side of the mountain, an anticyclonic bend over the highest part of the ridge, and again a cyclonic bend on the lee side. At higher levels, there is just an anticyclonic bend over the ridge.

10. Concluding remarks. The present study gives an indication of the structure and amplitude of the meso-scale inertia-gravity mountain wave in the two-dimensional case. The study is considered as tentative, however, since there are many features of the motion which could not be studied, such as the occurrence of critical waves (of wave length $2\pi U/f$), or wave guides bounded above by layers of low wind velocity which give rise to total reflection. In order to investigate such phenomena, it would be desirable to repeat the integrations for a region with considerably larger vertical and downstream extent.

REFERENCES

ELIASSEN, A. & PALM, E. 1961: On the transfer of energy in stationary mountain waves. *Geof. Publ. XII*, No. 3.

ELIASSEN, A. 1968: On meso-scale mountain waves on the rotating earth. *Geof. Publ. XXVII*, No. 6.

JONES, W. L. 1967: Propagation of internal gravity waves in fluids with shear and rotation. *J. Fluid Mech.* 30, p. 439.

NITTA, T. 1962: The outflow boundary condition in numerical time integration of advective equations. *J. Meteor. Soc. Japan*, Ser. II, 40, p. 13.

Papers published in *Geofysiske Publikasjoner* may be obtained from: Universitetsforlaget, Blindern, Oslo 3, Norway.

Vol. XXIII.

No. 1. Bernt Mæhlum: The sporadic E auroral zone. 1962.
» 2. Bernt Mæhlum: Small scale structure and drift in the sporadic E layer as observed in the auroral zone. 1962.
» 3. L. Harang and K. Malmjord: Determination of drift movements of the ionosphere at high latitudes from radio star scintillations. 1962.
» 4. Eyvind Riis: The stability of Couette-flow in non-stratified and stratified viscous fluids. 1962.
» 5. E. Frogner: Temperature changes on a large scale in the arctic winter stratosphere and their probable effects on the tropospheric circulation. 1962.
» 6. Odd H. Sælen: Studies in the Norwegian Atlantic Current. Part II: Investigations during the years 1954—59 in an area west of Stad. 1963.

Vol. XXIV.

In memory of Vilhelm Bjerknes on the 100th anniversary of his birth. 1962.

Vol. XXV.

No. 1. Kaare Pedersen: On the quantitative precipitation forecasting with a quasi-geostrophic model. 1963.
» 2. Peter Thrane: Perturbations in a baroclinic model atmosphere. 1963.
» 3. Eigil Hesstvedt: On the water vapor content in the high atmosphere. 1964.
» 4. Torbjørn Ellingsen: On periodic motions of an ideal fluid with an elastic boundary. 1964.
» 5. Jonas Ekman Fjeldstad: Internal waves of tidal origin. 1964.
» 6. A. Eftestøl and A. Omholt: Studies on the excitation of N_2 and N_2^+ bands in aurora. 1965.

Vol. XXVI.

No. 1. Eigil Hesstvedt: Some characteristics of the oxygen-hydrogen atmosphere. 1965.
» 2. William Blumen: A random model of momentum flux by mountain waves. 1965.
» 3. K. M. Storetvedt: Remanent magnetization of some dolerite intrusions in the Egersund Area, Southern Norway. 1966.
» 4. Martin Mork: The generation of surface waves by wind and their propagation from a storm area. 1966.
» 5. Jack Nordø: The vertical structure of the atmosphere. 1965.
» 6. Alv Egeland and Anders Omholt: Carl Størmer's height measurements of aurora. 1966.
» 7. Gunnvald Bøyum: The energy exchange between sea and atmosphere at ocean weather stations M, I and A. 1966.
» 8. Torbjørn Ellingsen and Enok Palm: The energy transfer from submarine seismic waves to the ocean. 1966.
» 9. Torkild Carstens: Experiments with supercooling and ice formation in flowing water. 1966.
» 10. Jørgen Holmboe: On the instability of stratified shear flow. 1966.
» 11. Lawrence H. Larsen: Flow over obstacles of finite amplitude. 1966.

Vol. XXVII.

No. 1. Arne Grammeltvedt: On the nonlinear computational instability of the equations of one-dimensional flow. 1967.
» 2. Jørgen Holmboe: Instability of three-layer models in the atmosphere. 1968.
» 3. Einar Høiland and Eyvind Riis: On the stability of shear flow of a stratified fluid. 1968.
» 4. Eigil Hesstvedt: On the effect of vertical eddy transport on atmospheric composition in the mesosphere and lower thermosphere. 1968.
» 5. Eigil Hesstvedt: On the photochemistry of ozone in the ozone layer. 1968.
» 6. Arnt Eliassen: On meso-scale mountain waves on the rotating earth. 1968.
» 7. Kaare Pedersen and Knut Erik Grønskei: A method of initialization for dynamical weather forecasting, and a balanced model. 1969.

A.s John Griegs Boktrykkeri